RSC Advances

PAPER

View Article Online
View Journal | View Issue

Cite this: *RSC Adv.*, 2016, **6**, 43152

Bifunctional Brønsted–Lewis solid acid as a recyclable catalyst for conversion of glucose to 5-hydroxymethylfurfural and its hydrophobicity effect†

Xuepeng Wang, Haijuan Zhang, Jingzhong Ma and Zhong-Hua Ma*

Received 7th February 2016
Accepted 19th April 2016

DOI: 10.1039/c6ra03565e

www.rsc.org/advances

A novel polydivinylbenzene polymeric material containing water-tolerant $SO_2NHSO_2C_4F_9$ with 2 equivalents of Cr(III) was explored as a catalyst of the one-pot conversion of glucose to 5-hydroxymethylfurfural (HMF) in a biphasic system. Stable 59–57% yields of HMF were achieved throughout 12 cycles over the bifunctional material. Dynamic analysis showed that Cr(III) essentially promoted the isomerization process of glucose to fructose. The material featured integral hydrophobicity, which, with the water-tolerance of $SO_2NHSO_2C_4F_9$, contributed to its excellent recyclability.

1. Introduction

Sustainable biomass resources are imaged to be a perfect solution to the crisis of increasing depletion of fossil fuel. The richest biomass, cellulose, will promisingly produce various building blocks, which are traditionally from fossil fuel and widely applied to high-value chemicals, biofuels and materials.

Glucose (Glu) is universally recognized as an important basic structural unit of cellulose. The transformation of Glu has thus always been attractive in recent years. A derivative platform product is 5-hydroxymethylfurfural (HMF), which is a precursor molecule of various building blocks. The Glu-to-HMF transformation includes two steps: Glu is isomerized into fructose (Fru) with Lewis acid or base catalysts; the cascade dehydration of Fru over acid catalyst provides HMF. Both the hexoses (Glu and Fru) contain highly active –OH and –C=O groups, which will easily incur complicated reactions. This brings a real challenge to the selective conversion of Glu over chemical catalysts with miscellaneous by-reactions compressed. Both base and acid are described to work on Glu-to-Fru transformation, and Brønsted acid has been reported to be superior.[1]

The synergistic relation between Brønsted acid and Lewis acid can promote a one-pot Glu conversion to HMF,[2–4] and further lactic derivatives,[5] levulinate,[3,6] *etc.* HMF is considered as a versatile platform chemical.

Reported Lewis acids include Cr(III), Al(III),[7] Cr(II), Zn(II),[8] Sn(IV), In(III),[9] and boric acid.[10] A strategy to prevent HMF from further degrading lies in real-time removal of HMF from aqueous mixtures with organic solvents (bi-phase extraction), preventing HMF from coming into contact with catalysts in water and thus improving the HMF yield.[11] The prevalent organic solvents include MIBK/butanol, THF, 2-*sec*-butylphenol. For example, one-pot catalysis gave HMF yields of 59% with $CrCl_3$/HCl in THF/H_2O,[3] and 62% with $AlCl_3$/HCl in alkylphenol/H_2O.[12] However, HMF selectivity was reported to be dependent on the reaction media.

Homogeneous catalysis systems unavoidably produce waste and erosion, driving the development of heterogeneous catalysts. Several promising silica-based bifunctional acid catalysts have been explored for one-pot conversion of hexoses.[13] Beta zeolite containing framework Sn atoms was highlighted as highly acid-tolerant, and applicable to Glu-to-Fru isomerization in water.[14–16] This allowed the one-pot Glu-to-HMF conversion through a cascade reaction sequence involving isomerization and dehydration. Lewis acid sites confined in hydrophobic pockets have been utilized as structural motifs contributing to turnover rate enhancement.[17] Besides, hybrid catalysts with $CrCl_3$ and HY zeolite catalysed the conversion of Glu-to-levulinic acid with a 62% yield.[18] Hybrid carbon–silica catalysts, grafting the silica with Sn(IV) and filling with a carbon network, provided weak Brønsted acid and Lewis acid for lactate formation from hexoses and disaccharides.[5]

Functionalized mesoporous silica is another popular silica-based catalyst, and silica is subject to the stability headache owing to siloxane bond breakage in hot liquid water.[19,20] However, for effective conversion of monosaccharides into platform molecules or building blocks, increasing the severity of the aqueous media is often requested. This is despite the fact that monosaccharide bond breakage is efficiently carried out in

Department of Chemistry, College of Sciences, Huazhong Agricultural University, Wuhan 430070, PR China. E-mail: mazonghua@mail.hzau.edu.cn

† Electronic supplementary information (ESI) available. See DOI: 10.1039/c6ra03565e

aqueous media. Ionization of water increases with the increase of temperature, so that increased H^+ and OH^- ions would adhere to the surface of the support and possibly corrode the silica matrix. However, water acts as a non-substitutable solvent in the conversion of hexoses in order to meet solubility requirement, and sometimes coordinates the active Lewis acid centres.[15,17]

One way to improve the water-tolerance of catalysts is to improve their hydrophobicity, helpfully resisting against the adherence of hot liquid water;[20–24] and provide better wettability to organic substrates, which increases the catalytic efficiency.[2,20,24–26] The cooperation of superhydrophobic solid acid and superhydrophilic solid base catalysts has led to yields of HMF as high as 95.4% for one-pot conversion of glucose owing to the unique wettability of the combined catalyst.[2] To the best of our knowledge, this is the highest HMF yield so far.

Recently, SO_3H-functionalized polymeric ionic liquids containing Cr(III) provided a HMF yield of 48.7% from Glu.[27] Chromium(III) Schiff base complexes and acidic ionic liquids immobilized on mesoporous silica provided a HMF yield of 43.5% from Glu.[4] Selectivity research indicated that Glu conversion in water was highly dependent on the ratio of Brønsted acid to Lewis acid.[28]

SO_3H-resin is always favoured due to its commerciality and efficient performance in catalysis. However, for most traditional SO_3H-resins, the decomposition happens above 120 °C. As mentioned above, increasing the severity is often requested for efficient conversion of monosaccharides, including increased reaction temperature, which probably causes the weakness of the recyclability of solid acids. Research on practically water-tolerant solid acids with good recyclability thus intrigued us in recent years. Herein, we reported new types of supported bifunctional solid acids, using fluoroalkyl sulfonyl imide instead of an SO_3H group to provide Brønsted acid sites, while Cr(III) was bonded as a Lewis acid. The alternate Brønsted acid possesses outstanding thermal stability and strong gas-phase acidity.[29–31] Hydrophobic poly-divinylbenzene (PDVB) polymer and hydrophilic silica (SiO_2) were used as supports for comparison. PDVB polymer and the water-tolerant fluoroalkyl sulfonyl imide groups together contribute to excellent catalyst longevity in a hot aqueous methyl isobutyl ketone (MIBK) biphasic system of Glu-to-HMF conversion, recycling 12 times with a stable Glu conversion and HMF production.

2. Experimental

2.1 Chemicals and materials

The chemicals include $CrCl_3 \cdot 6H_2O$, glucose, fructose, H_2O_2, HMF, MIBK, and BuOH. All materials were purchased in reagent grade and used as such. Solvents (A. R.) for synthesis were commercially available in China. NKC-9, a SO_3H-style resin with polystyrene as the support, was acidified with 5–10% HCl followed by water scrubbing to remove Cl^-. After vacuum drying at 80 °C for 24 h, the resin contained 4.6 mmol g^{-1} Brønsted acid and 10 wt% combined water determined experimentally (Tianjin Nankai Chemical).

2.2 Characterization

Chromium loadings were determined on an AMPTEK X-123 X-ray fluorescence (XRF) spectrometer with a 30 eV and 100 mA generator. Energy ranges of Cr(III) are between 5.14 and 5.56 ekV. Transmission electron microscopy (TEM) images were recorded on a Tecnai G2 20 microscope at an accelerating voltage of 300 kV. The textural properties of the samples were measured on ASAP2460 using the BET procedure, and the mesopore size distribution was obtained using the BJH methods with desorption branch. Pyridine-FT-IR spectra were obtained on an Avatar 330 Fourier Spectrometer with the KBr pellet technique, the samples pre-absorbed with pyridine adequately under vacuum at 50 °C, and excess pyridine was blown off with N_2 flow. Thermogravimetric analysis (TGA) was carried out on a TG209 (Netzsch) under air atmosphere from room temperature to 700 °C with a ramp of 20 °C min^{-1}. Contact angles of water were performed on a SL200KB contact angle measuring system equipped with a CCD camera. The static contact angles were measured in sessile drop mode. HMF and carbohydrates were analyzed on an Agilent 1200 Series, equipped with a VWD and RID Detector. An XDB-C18 reversed-phase column (150 mm × 4.6 mm, 5 μm) was used for HMF and a Ca-NP10 column (7.8 × 300 mm, 10 μm) for carbohydrates.

2.3 Synthesis of bifunctional solid acids

Solid Brønsted acids, H-PDVB-0.3-SSFBI and H-PSFSI-$MSMA_{15}$/SiO_2 (Fig. 1), were synthesized according to literature ref. 24 and 29, respectively. H-PDVB-0.3-SSFBI possesses phenylsulfonyl perfluorobutylsulfonyl imide groups ($PhSO_2NHSO_2C_4F_9$) with hydrophobic PDVB support (0.79 mmol g^{-1}, D_{BJH} 3.81 nm, S_{BET} 346 m^2 g^{-1}, V_{total} 0.25 cm^3 g^{-1}); H-PSFSI-$MSMA_{15}$/SiO_2 possesses the same $SO_2NHSO_2C_4F_9$ groups, but with hydrophilic SiO_2 support (0.66 mmol g^{-1}, D_{BJH} 3.83 nm, S_{BET} 233 m^2 g^{-1}, V_{total} 0.38 cm^3 g^{-1}).

The preparation of bifunctional solid acids was carried out by cationic exchange. Solid Brønsted acid (*ca.* 6 g) was added into 400 mL of distilled water and $CrCl_3 \cdot 6H_2O$ was added in batches with stirring. The pH value of the mixture was monitored by pH meter in real time, and decreased with the exchange of Cr^{3+} and H. The exchange capacity was obtained by calculation of the concentration of H^+ in the solution. The varying pH value suggested the controllable exchange capacity. Generally, the molar ratio of loaded Cr(III) : H on the resulting bifunctional solid acids was optimized as 2 : 1. Acid remains were removed with distilled water. The loading of Cr(III) was further confirmed by XRF.

Typically, 6.19 g of H-PDVB-0.3-SSFBI and 1.96 g of $CrCl_3 \cdot 6H_2O$ were used. The pH value varied until around 1.98, and the obtained bifunctional solid acid was denoted as Cr(III)-

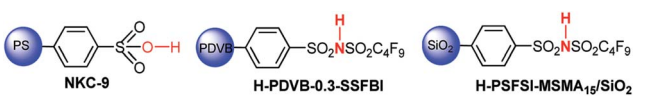

Fig. 1 Chemical structures of solid Brønsted acids.

PDVB-0.3-SSFBI. Additionally, 5.33 g of NKC-9 and 5.98 g of $CrCl_3 \cdot 6H_2O$ were used for the preparation of Cr(III)-NKC-9, and the pH value was 1.29, while 6.35 g of H-PSFSI-$MSMA_{15}/SiO_2$ and 1.22 g of $CrCl_3 \cdot 6H_2O$ were used for Cr(III)-PSFSI-$MSMA_{15}/SiO_2$ with the pH at 2.05.

2.4 Measurement of acid loadings of bifunctional solid acids

The Cr(III) loadings of bifunctional solid acids were determined by XRF analysis (see ESI†) while the Brønsted acid loadings were obtained by subtraction of stoichiometric hydrogen of the corresponding molar numbers of Cr(III) from the initial Brønsted acid loadings of solid Brønsted acids (H-PDVB-0.3-SSFBI, H-PSFSI-$MSMA_{15}/SiO_2$ and NKC-9), which were determined by titration with NaOH.[22] The Brønsted acid loadings of bifunctional solid acids were further verified by pH meter.

2.5 Catalytic testing

All catalyst evaluations were conducted in a 20 mL autoclave with a magnetic stirring bar. Reactions were carried out in triplicate at 140 °C using 1.5 mL of 5 wt% glucose or fructose solution plus 0.5 mL of DMSO as the aqueous phase, and 9.8 mL of MIBK plus 4.2 mL of butanol as the organic phase (7 : 3). The optimized volume ratio of aqueous and organic phases (V_{H_2O} : V_{org}) was 1 : 7. The molar ratios of Cr(III) of the catalysts to Glu were 3 : 10. Reactions were quenched in turn by water-cooling every 30 minutes. HPLC conversions/yields were obtained based on both aqueous and organic phase analysis.

The transformation experiments of HMF (0.35 wt%) were carried out in MIBK/butanol solvent, and no water/DMSO was added.

Recovered bifunctional solid acids were treated with H_2O_2 for 5 hours at 40 °C to restore to blue from brown or black, and reused in the next cycle.

3. Results and discussion

3.1 Synthesis and characterization of bifunctional solid acids

Three solid Brønsted acids, NKC-9, H-PDVB-0.3-SSFBI, and H-PSFSI-$MSMA_{15}/SiO_2$, are illustrated in Fig. 1. Their acid sites were partially exchanged by Cr^{3+} to introduce Lewis acid sites Cr(III), and produce bifunctional solid acids. Both the acid sites co-catalysed the hydrolysis of Glu.

The loadings of Cr(III) are dependent on the feeding of $CrCl_3 \cdot 6H_2O$. The change of concentration of Cr^{3+} can be worked out by pH value, which is monitored conveniently using a pH meter. The obtained results are further confirmed with XRF analysis as molar ratios of Cr(III)/H^+ equal to 1.9, 2.1 and 1.8, respectively for Cr(III)-NKC-9, Cr(III)-PDVB-0.3-SSFBI and Cr(III)-PSFSI-$MSMA_{15}/SiO_2$. The XRF spectra are shown in Fig. 2.

Pyridine-FT-IR spectra (Fig. 3) further show the presence of both the acid sites. The solid Brønsted acids give clear bonds at 1541 cm^{-1}, which are generally considered as stretching vibrations of C–N of pyridine with a hydrogen proton absorbed. This peak appears weaker for PDVB-0.3-SSFBI owing to lower Brønsted acid loadings. Peaks at 1450 cm^{-1} are assigned to the

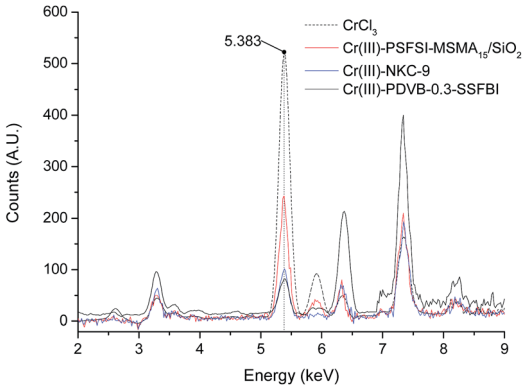

Fig. 2 XRF spectra of bifunctional solid acids and $CrCl_3$.

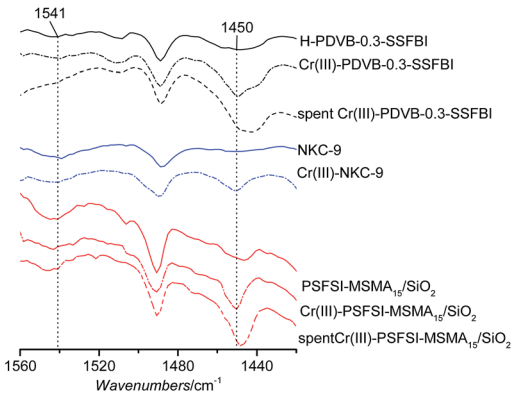

Fig. 3 Pyridine-FT-IR spectra of various fresh/spent bifunctional solid acids.

C–C(N) characteristic vibration of pyridine combined with Lewis acid sites, which is phenomenally strengthened for three bifunctional solid acids, suggesting the increase of Cr(III) loadings. The distributions of Cr and F of Cr(III)-PDVB-0.3-SSFBI were investigated by EDX using STEM mode, as shown in Fig. 4(a–c). Both Cr and F were readily detectable with homogeneous distributions, suggesting homogeneous distributions of fluoroalkyl sulfonyl imide and Cr(III) in the materials. The particles were amorphous, judging by the fringe disorder shown in Fig. 4(a). Additionally, S, O, N and C were also detectable with homogeneous distributions, shown in Fig. S2.†

The nitrogen adsorption–desorption isotherms of the bifunctional solid acids are shown in Fig. 5 and S3.† Typical type IV isotherms, characteristic of mesoporous materials, appear for Cr(III)-PDVB-0.3-SSFBI (Fig. 5(a)) and Cr(III)-PSFSI-$MSMA_{15}/SiO_2$ (Fig. S3(c)†). A hysteresis loop was observed clearly at low relative pressure (0.45–0.95) and broadly, suggesting the dominant mesoporous structure but non-uniform pore size distribution. Both Cr(III)-PDVB-0.3-SSFBI and Cr(III)-PSFSI-$MSMA_{15}/SiO_2$ show us rich disordered pores, which is in reasonable agreement with the results from TEM images. Their pore networks are irregular. For Cr(III)-NKC-9, a type III isotherm is observed, suggesting a non-porous structure (Fig. S3†). The BET surface area and pore volume are listed in

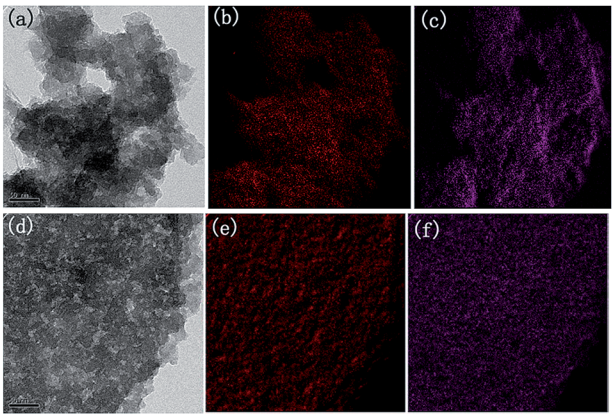

Fig. 4 Representative TEM images and elemental maps of fresh (a–c) and spent (d–f) Cr(III)-PDVB-0.3-SSFBI. (b) and (e) are EDX maps of Cr; (c) and (f) are maps of F.

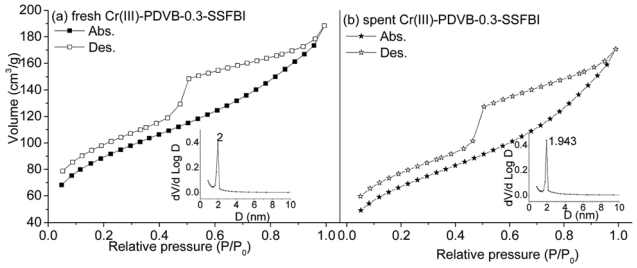

Fig. 5 N_2 adsorption–desorption isotherms of fresh (a) and spent (b) Cr(III)-PDVB-0.3-SSFBI, and BJH mesopore size distribution from desorption branch (inset).

Table S2.† The higher surface area (>230 $m^2\ g^{-1}$) and larger pore volume (>0.24 $cm^3\ g^{-1}$) are achieved for Cr(III)-PDVB-0.3-SSFBI and Cr(III)-MSMA$_{15}$/SiO$_2$, but only 25 $m^2\ g^{-1}$ and 0.032 $cm^3\ g^{-1}$ for Cr(III)-NKC-9.

TG analysis is shown in Fig. 6 and S4.† The mass-loss of 0.2%, 3% and 3.7% occurs to Cr(III)-PDVB-0.3-SSFBI, Cr(III)-PSFSI-MSMA$_{15}$/SiO$_2$ and Cr(III)-NKC-9 below 100 °C, respectively, which can reasonably be attributed to incorporated water (Fig. 6). Subsequently, a minor mass-loss happens to Cr(III)-PDVB-0.3-SSFBI (2%) and Cr(III)-PSFSI-MSMA$_{15}$/SiO$_2$ (4%) from

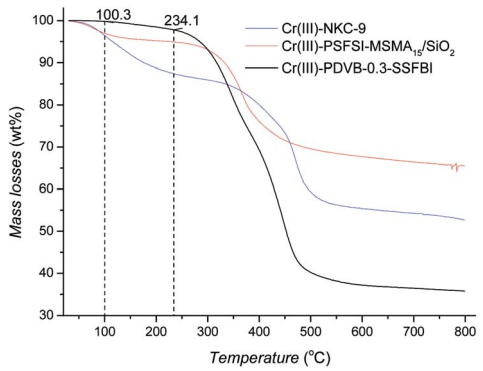

Fig. 6 TG analysis of various bifunctional solid acids.

100 to 234 °C; while a large mass-loss of *ca.* 8% of Cr(III)-NKC-9 appears continuously. A similar tendency occurs to the corresponding solid Brønsted acids (Fig. S4†), negligible for H-PDVB-0.3-SSFBI and H-PSFSI-MSMA$_{15}$/SiO$_2$ from 100 to 150 °C, but significant 5% for NKC-9. The mass-loss is mainly owing to incorporated water, which remained after vacuum drying at the moderate temperature.[32] It is thus inferred that the mass-loss of 8% of Cr(III)-NKC-9 is inclusive of the evaporation of incorporated water and probably the additional dehydration of coordinative hydroxyls of Cr(III). Despite no further definite evidence, better hydrothermal stability would be expected for Cr(III)-PDVB-0.3-SSFBI owing to the much lower mass-loss.[24]

3.2 Catalytic performance

All three bifunctional solid acids effectively catalysed the Glu conversion into HMF in a biphasic system. In the system, DMSO was used to depress formation of levulinic acid and humins, and MIBK was used to extract HMF from the water phase.[11] As shown in Fig. 7(a), Cr(III)-NKC-9 and Cr(III)-PSFSI-MSMA$_{15}$/SiO$_2$ gave nearly 100% conversion and 62–67% yield of HMF within 4 hours, while Cr(III)-PDVB-0.3-SSFBI gave comparable 94% and 60% within 7 hours. With solid Brønsted acids (Fig. 7(b)), <60% conversion of Glu within 7 hours and <35% yield of HMF within 10 hours were given. The deficiency of Cr(III) of solid Brønsted acids thus underlay the decreases of Glu conversions and HMF yields.

The Glu conversion catalysed by acid was reported as a pseudo first order reaction. Here, the calculated rate constants of the Glu conversion are $k_{NKC} = 0.9142\ h^{-1}$, $k_{SiO_2} = 0.8921\ h^{-1}$, and $k_{PDVB} = 0.3369\ h^{-1}$, respectively, for Cr(III)-NKC-9, Cr(III)-PSFSI-MSMA$_{15}$/SiO$_2$, and Cr(III)-PDVB-0.3-SSFBI (Fig. 8(a)). The conversion to HMF also includes the subsequent Fru-to-HMF dehydration (Fig. 7(c)). The rate constants of the Fru dehydration are remarkably higher at $k'_{NKC} = 1.5720\ h^{-1}$, $k'_{SiO_2} = 1.5040\ h^{-1}$, and $k'_{PDVB} = 1.1780\ h^{-1}$ (Fig. 8(c)). The Glu isomerization is thus the slower of the two steps, mainly limiting the apparent

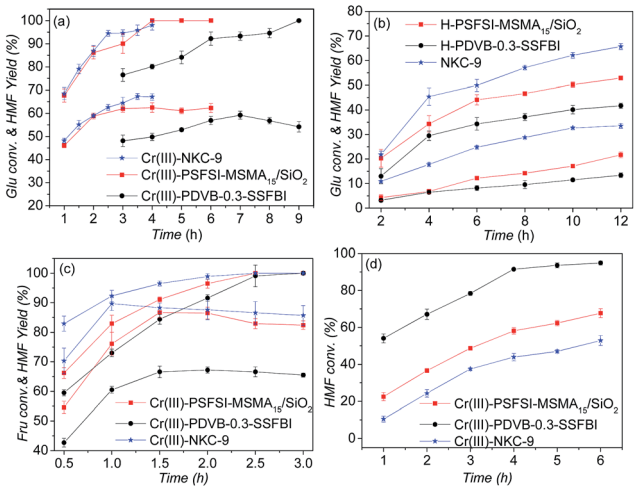

Fig. 7 Various acid materials-catalysed conversions of glucose (a and b), fructose (c), and HMF (d).

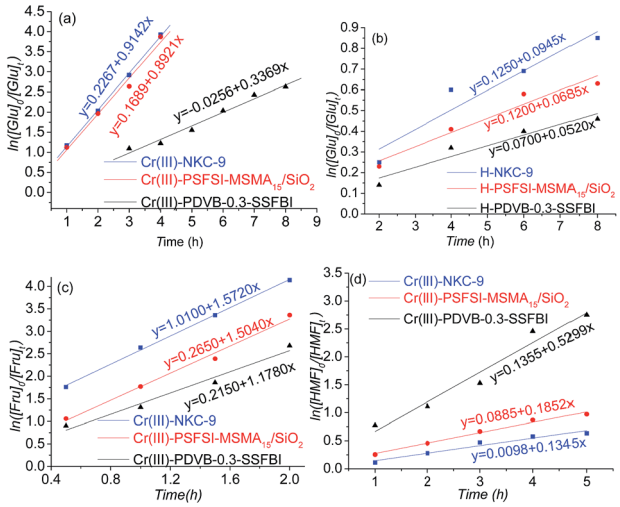

Fig. 8 Rate constants of Glu-to-HMF conversion over various acid materials. (a and b) Glu conversion; (c) Fru conversion; and (d) HMF conversion.

rates of the Glu-to-HMF conversion catalysed by bifunctional solid acids.

In order to clarify the effect of the Cr(III) of the bifunctional solid acids on the Glu isomerization, the three solid Brønsted acids, which have no Cr(III) loaded, were used to catalyse Glu conversions. The rate constants were 0.0945 h^{-1}, 0.0685 h^{-1} and 0.0520 h^{-1}, respectively for NKC-9, H-PSFSI-MSMA$_{15}$/SiO$_2$, and H-PDVB-0.3-SSFBI, an order of magnitude lower than those of the bifunctional solid acids. The rates slow down significantly owing to the deficiency of Cr(III), the Lewis acid site. Cr(III) is thus believed to play a key role in isomerizing Glu to Fru.

The rate constants of Glu conversion of the bifunctional solid acids are compared in a ratio as $k_{NKC} : k_{SiO_2} : k_{PDVB} = 2.71 : 2.65 : 1$, while the ratio of the rate constants of the subsequent dehydration is $k'_{NKC} : k'_{SiO_2} : k'_{PDVB} = 1.33 : 1.28 : 1$. The more discriminant ratio of Glu conversion suggests that Cr(III)-NKC-9 and Cr(III)-PSFSI-MSMA$_{15}$/SiO$_2$ promoted the isomerization process more efficiently, and Cr(III)-PDVB-0.3-SSFBI gave a comparable promotion effect just on the subsequent dehydration, giving the about equal rate constants.

The difference of rate constants k_{SiO_2} and k_{PDVB} indicates the support effect of the different catalysts on the isomerization. Although induced by the same acid sites ($SO_2NHSO_2C_4F_9$ and Cr(III)), k_{SiO_2} is much larger than k_{PDVB} (2.65 : 1). This difference is attributed to the different properties of the SiO_2 and PDVB supports. Additionally, k_{NKC} is a description of the catalytic effect of SO_3H, but is close to k_{SiO_2} (2.71 : 2.65). No obvious observations showed the influence of different Brønsted acid sites on Glu conversion rates.

A relatively fast degradation of HMF catalysed by Cr(III)-PDVB-0.3-SSFBI was observed (Fig. 7(d) and 8(d)). The rate constants of HMF degradation were 0.1345, 0.1852, and 0.5299, respectively for Cr(III)-NKC-9, Cr(III)-PSFSI-MSMA$_{15}$/SiO$_2$ and Cr(III)-PDVB-0.3-SSFBI. This can explain the slightly lower HMF yield maximum (60%) and longer required reaction time (7 h) (Fig. 7(a)).

As discussed above in TG analysis, Cr(III)-PDVB-0.3-SSFBI prevents the adherence of water, for which the integral hydrophobicity of the material could provide an explanation (Fig. 9). The contact angle of water of Cr(III)-PDVB-0.3-SSFBI is 109.8°, suggesting that hydrophobicity of the PDVB support is carried over into the bifunctional solid acid. Not surprisingly, the other two bifunctional solid acids give low angles of 24.0° and 41.4°, respectively. Of note, the hydrophobicity of PS support of Cr(III)-NKC-9 is slackened by high acid density, inherently switching into the integral hydrophilicity.

On the other hand, the hydrophilic catalysts, Cr(III)-NKC-9 and Cr(III)-PSFSI-MSMA$_{15}$/SiO$_2$, would be more accessible to the intrinsically hydrophilic Glu molecules, helping to absorb Glu and promoting its conversion. This can explain why k_{NKC} and k_{SiO_2} are much higher than k_{PDVB}. However, the reaction systems were split into two phases at room temperature—organic layer (upper layer) and water layer (bottom layer). As shown by the insets in Fig. 9, Cr(III)-PDVB-0.3-SSFBI was in the upper layer, and the other two were in the bottom layer. Experimentally, Cr(III)-PDVB-0.3-SSFBI was resistant to water. Better hydrothermal stability of Cr(III)-PDVB-0.3-SSFBI was thus expected.

Recovered bifunctional solid acids were re-activated with hydrogen peroxide and recycled in subsequent reactions. Hydrogen peroxide was believed to oxidize and solve dark-color by-products. Cr(III)-NKC-9 gave a dramatically decreased Glu conversion (97 to 60%) and HMF yield (65 to 41%), along with poor catalyst recovery (Fig. 10). After 4 cycles, Cr(III)-NKC-9 became too sticky to get recovered. A similar situation happened to Cr(III)-PSFSI-MSMA$_{15}$/SiO$_2$, becoming sticky after 7 cycles with reduced HMF yield (62 to 53%). The results were comparable to the recently reported 43.5% HMF yield and 5 cycles of reusability catalysed by novel chromium(III) Schiff base complexes and acidic ionic liquids immobilized on mesoporous silica.[4] Excitingly, Cr(III)-PDVB-0.3-SSFBI mediated the transformation with a stable conversion of 95–85% and a HMF yield of 59–57% up to 12 cycles. After 12 cycles of reactions, the amount of recovered catalyst was too little to ensure accurate experimental results.

Nevertheless, the recovered Cr(III)-PDVB-0.3-SSFBI and Cr(III)-PSFSI-MSMA$_{15}$/SiO$_2$ (Fig. 3) still gave clear signals at 1450 and 1541 cm^{-1}, and both Cr and F were still detectable for Cr(III)-PDVB-0.3-SSFBI with homogeneous distributions by EDX using STEM mode (Fig. 4(d–f)), suggesting that bifunctional acid sites were maintained. Two spent imide-style

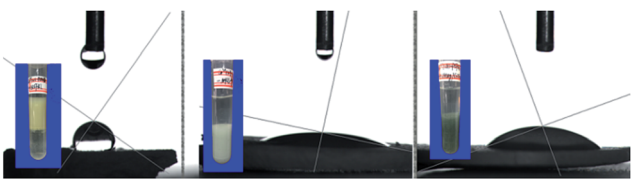

Fig. 9 Contact angles of water droplets on the surface of bifunctional solid acids and distribution of the catalysts in a biphasic system (insets). Cr(III)-PDVB-0.3-SSFBI (left, 109.8°), Cr(III)-NKC-9 (middle, 24.0°), and Cr(III)-PSFSI-MSMA$_{15}$/SiO$_2$ (right, 41.4°).

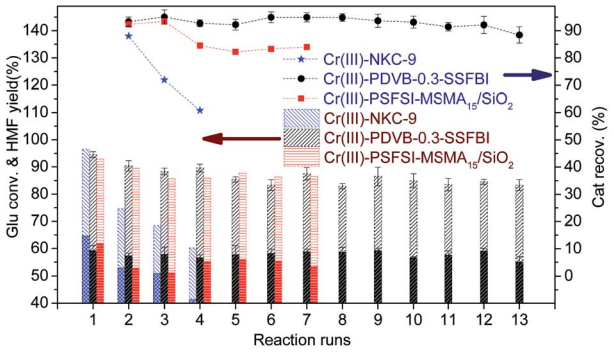

Fig. 10 Cycle lives of bifunctional solid acids in Glu-to-HMF conversion in biphasic systems.

catalysts were still characteristic of stable mesoporous structure with a typical IV isotherm by N_2 adsorption–desorption (Fig. 5(b) and S3(d)†).

The reusability of Cr(III)-PDVB-0.3-SSFBI was superior to that of the other two, which was attributed to its more excellent integral hydrophobicity. The integral hydrophobicity is advantageous in mediating organic reactions in water-containing systems aided by water-tolerable $PhSO_2NHSO_2C_4F_9$ groups.[24] At the same time, the hydrophobic surrounding environment does not block the Lewis acid sites' access to water molecules,[17] ensuring that the Glu isomerization performed smoothly. Cr(III)-NKC-9 has hydrophobic support PS and all-organic ingredients, but the hydroscopicity of the acid groups undesirably leads to integral hydrophilicity. No direct evidence is given to suspect the thermal stability of $-SO_3H$ groups in the reactions, but the remarkable superior recyclability of Cr(III)-PSFSI-$MSMA_{15}/SiO_2$ (up to 7 cycles) to Cr(III)-NKC-9, both are hydrophilic, should be attributed to the improvement of the stability of the $PhSO_2NHSO_2C_4F_9$ group. Thus, the excellent recyclability of Cr(III)-PDVB-0.3-SSFBI is attributed to the combination of water-tolerant $PhSO_2NHSO_2C_4F_9$ groups and integral hydrophobicity.

4. Conclusions

A practical one-pot protocol was developed for converting glucose to 5-hydroxymethylfurfural (HMF) by employing a new type of bifunctional solid acid. The materials contain strong Brønsted acid and Cr(III) Lewis acid, and Cr(III) essentially isomerized glucose to fructose. The catalytic efficacy relied on the integral hydrophobicity of the catalysts. Hydrophilic catalysts acted more efficiently at the expense of cycle life, while hydrophobic catalyst Cr(III)-PDVB-0.3-SSFBI maintained high efficiency in the continuous 12-cycles conversion based on easy regeneration, providing 95–85% conversion and 59–57% HMF yield. Cr(III) Lewis acid sites primarily promoted the isomerization of Glu-to-Fru. The integral hydrophobicity of Cr(III)-PDVB-0.3-SSFBI, along with water-tolerant $PhSO_2NHSO_2C_4F_9$ groups, together contributed to good cycle longevity. Further extension of this type of materials into other reactions is underway.

Acknowledgements

We gratefully acknowledge the National Science Foundation of China (No. 21172083) and the Fundamental Research Funds for the Central Universities (No. 2662015PY060).

References

1 Y. Roman-Leshkov and M. E. Davis, *ACS Catal.*, 2011, **1**, 1566–1580.
2 L. Wang, H. Wang, F. J. Liu, A. M. Zheng, J. Zhang, Q. Sun, J. P. Lewis, L. F. Zhu, X. J. Meng and F. S. Xiao, *ChemSusChem*, 2014, **7**, 402–406.
3 V. Choudhary, S. H. Mushrif, C. Ho, A. Anderko, V. Nikolakis, N. S. Marinkovic, A. I. Frenkel, S. I. Sandler and D. G. Vlachos, *J. Am. Chem. Soc.*, 2013, **135**, 3997–4006.
4 Y. Wang, Z. Gu, W. Liu, Y. Yao, H. Wang, X.-F. Xia and W. Li, *RSC Adv.*, 2015, **5**, 60736–60744.
5 F. de Clippel, M. Dusselier, R. Van Rompaey, P. Vanelderen, J. Dijkmans, E. Makshina, L. Giebeler, S. Oswald, G. V. Baron, J. F. M. Denayer, P. P. Pescarmona, P. A. Jacobs and B. F. Sels, *J. Am. Chem. Soc.*, 2012, **134**, 10089–10101.
6 V. B. Kumar, I. N. Pulidindia and A. Gedanken, *RSC Adv.*, 2015, **5**, 11043–11048.
7 S. De, S. Dutta and B. Saha, *Green Chem.*, 2011, **13**, 2859–2868.
8 C. B. Rasrendra, I. G. B. N. Makertihartha, S. Adisasmito and H. J. Heeres, *Top. Catal.*, 2010, **53**, 1241–1247.
9 Y. Shen, J. K. Sun, Y. X. Yi, M. F. Li, B. Wang, F. Xu and R. C. Sun, *Bioresour. Technol.*, 2014, **172**, 457–460.
10 T. Stahlberg, S. Rodriguez-Rodriguez, P. Fristrup and A. Riisager, *Chem.–Eur. J.*, 2011, **17**, 1456–1464.
11 Y. Roman-Leshkov, J. N. Chheda and J. A. Dumesic, *Science*, 2006, **312**, 1933–1937.
12 Y. J. Pagan-Torres, T. F. Wang, J. M. R. Gallo, B. H. Shanks and J. A. Dumesic, *ACS Catal.*, 2012, **2**, 930–934.
13 J. B. dos Santos, N. Albuquerque, C. L. P. S. Zanta, M. R. Meneghetti and S. Plentz Meneghetti, *RSC Adv.*, 2015, **5**, 90952–90959.
14 M. Moliner, Y. Roman-Leshkov and M. E. Davis, *Proc. Natl. Acad. Sci. U. S. A.*, 2010, **107**, 6164–6168.
15 R. Bermejo-Deval, R. S. Assary, E. Nikolla, M. Moliner, Y. Roman-Leshkov, S. J. Hwang, A. Palsdottir, D. Silverman, R. F. Lobo, L. A. Curtiss and M. E. Davis, *Proc. Natl. Acad. Sci. U. S. A.*, 2012, **109**, 9727–9732.
16 N. Rai, S. Caratzoulas and D. G. Vlachos, *ACS Catal.*, 2013, **3**, 2294–2298.
17 R. Gounder and M. E. Davis, *J. Catal.*, 2013, **308**, 176–188.
18 N. Ya'aini, N. A. S. Amin and S. Endud, *Microporous Mesoporous Mater.*, 2013, **171**, 14–23.
19 H. F. Xiong, H. N. Pham and A. K. Datye, *Green Chem.*, 2014, **16**, 4627–4643.
20 R. Gounder, *Catal. Sci. Technol.*, 2014, **4**, 2877–2886.
21 F. Liu, A. Zheng, I. Noshadi and F.-S. Xiao, *Appl. Catal., B*, 2013, **136–137**, 193–201.

22 B. Chang, J. Fu, Y. Tian and X. Dong, *J. Phys. Chem. C*, 2013, **117**, 6252–6258.
23 P. A. Zapata, Y. Huang, M. A. Gonzalez-Borja and D. E. Resasco, *J. Catal.*, 2013, **308**, 82–97.
24 M. He, J. Xu, Z.-H. Ma, H. Yuan and J. Ma, *Microporous Mesoporous Mater.*, 2015, **211**, 30–37.
25 B. Karimi and M. Vafaeezadeh, *Chem. Commun.*, 2012, **48**, 3327–3329.
26 F. Liu, L. Wang, Q. Sun, L. Zhu, X. Meng and F.-S. Xiao, *J. Am. Chem. Soc.*, 2012, **134**, 16948–16950.
27 H. Li, Q. Zhang, X. Liu, F. Chang, Y. Zhang, W. Xue and S. Yang, *Bioresour. Technol.*, 2013, **144**, 21–27.
28 R. Weingarten, Y. T. Kim, G. A. Tompsett, A. Fernandez, K. S. Han, E. W. Hagaman, W. C. Conner, J. A. Dumesic and G. W. Huber, *J. Catal.*, 2013, **304**, 123–134.
29 Q.-H. Yang, Z.-H. Ma, J.-Z. Ma and J. Nie, *Microporous Mesoporous Mater.*, 2013, **172**, 51–60.
30 I. Leito, E. Raamat, A. Kütt, J. Saame, K. Kipper, I. A. Koppel, I. Koppel, M. Zhang, M. Mishima, L. M. Yagupolskii, R. Y. Garlyauskayte and A. A. Filatov, *J. Phys. Chem. A*, 2009, **113**, 8421–8424.
31 I. A. Koppel, R. W. Taft, F. Anvia, S.-Z. Zhu, L.-Q. Hu, K.-S. Sung, D. D. DesMarteau, L. M. Yagupolskii and Y. L. Yagupolskii, *J. Am. Chem. Soc.*, 1994, **116**, 3047–3057.
32 N. Bothe, F. Döscher, J. Klein and H. Widdecke, *Polymer*, 1979, **20**, 850–854.